Inverse stochastic resonance in electroconvection by multiplicative colored noise

Jong-Hoon Huh
Department of Mechanical Information Science and Technology, Faculty of Computer Science and Systems Engineering, Kyushu Institute of Technology, Fukuoka 820-8502, Japan
(Received 5 July 2016; published 8 November 2016)

A kind of inverse stochastic resonance (ISR) observed in ac-driven electroconvection (EC) in a nematic liquid crystal is presented. In successive pattern evolutions by increasing noise intensity V_N, a typical EC (with a normalized amplitude $A_0 = 1$ at $V_N = 0$) disappears ($A_0 \to 0$), and then the rest state ($A_0 = 0$) reenters into the EC ($A_0 = 1$); eventually, it develops into complicated EC($A_0 > 1$). The reversed bell-shaped behavior of $A_0(V_N)$ is evidence of ISR. The present ISR may be explained by taking into account colored noise characterized by its intensity and correlation time.

DOI: 10.1103/PhysRevE.94.052702

I. INTRODUCTION

Noise-related phenomena have been extensively investigated in various fields [1–3]. Generally, considering the fluctuations of material and/or control parameters in natural and artificial systems, noise (as the origin of the fluctuations) should be minimized for desirable treatments. Therefore, numerous efforts have been made for the minimization of noise so that great success could have been achieved in many cases [4,5]. Contrary to such a negative aspect of noise, however, constructive and productive noise has been appreciated in diverse systems for the last three decades [1–3,6,7]. In particular, stochastic resonance (SR) [8–10] must be one of the most important phenomena to trigger studies on noise in which it plays a crucial role in order control, phase transition, and output enhancement, etc. [9,10]. Most importantly, SR shows a maximal response with respect to an optimal noise level (with an intensity not too small and not too large). Therefore, the signal-noise rate (SNR) shows typical bell-shaped behavior in the function of noise intensity. Hence, it has been emphasized in many papers [8–10] that SR contributes to enhancement of the output of systems. For instance, an order parameter of a system shows the largest value at the optimal noise level.

Surprisingly, noise-intensity-dependent SNR showing a *minimal* response was recently found in nervous systems [11–15]. By analogy with SR, it has been called *inverse stochastic resonance* (ISR) [12–15]. In those central nervous systems, the rhythmic firing activity of neurons decreases with increasing noise intensity, and then shows *reversed bell-shaped* behavior; even noise-induced on-off switching between the repetitive firing and quiescence of neurons was found. To the best of our knowledge, ISR was experimentally observed only in those systems, and has been analyzed in the Hodgkin-Huxley model considering noise [11–15]; the original model describes the time evolution of the membrane potential in terms of ionic currents [16].

On the other hand, particular attention has been paid to the noise impact on spatially extended dynamical systems out of equilibrium such as Belousov-Zhabotinsky reaction systems and *Rayleigh-Bénard* convection systems [17–22]. In those systems threshold problems and pattern formations are markedly changed by noise; also, SR-like behavior was often found [17–19,22].

In this study, we address ac-driven electroconvection (EC) in nematic liquid crystals (NLCs) which have also been intensively studied for understanding the noise impact on spatially extended nonequilibrium systems [23–25]. The EC system has a rest state and a convection state below and above a threshold voltage, respectively; they may correspond to the quiescence and repetitive firing in nervous systems, respectively. Namely, it is an attractive system for investigating ISR in non-nervous systems. Our purpose is to present a kind of ISR discovered in the EC system by using *multiplicative colored noise*. Carefully controlling the intensity and correlation time of the noise, the EC system gives rise to ISR that has been overlooked in past research performed in unsuitable colored noise [23–25].

II. EXPERIMENT

First, to induce EC in the system, a sinusoidal ac field $\boldsymbol{E}(t) = \boldsymbol{E}\,[0, 0, E(t)]$ was applied across a thin slab [with a thickness $d = 50\,\mu$m and a lateral (active) size $L_x \times L_y = 1 \times 1\,\text{cm}^2$] of an NLC [$p$-methoxybenzylidene-$p'$-$n$-butylaniline (MBBA)] sandwiched between two parallel, transparent electrodes (indium tin oxide). The MBBA used in this study had the conductivity anisotropy $\sigma_a = 6.21 \times 10^{-8}\,\Omega^{-1}\,\text{m}^{-1}$ and dielectric anisotropy $\varepsilon_a = -0.35$. Next, to investigate the noise impact on EC, a Gaussian-type electric noise $\boldsymbol{\xi}(t) = \boldsymbol{\xi}[0,0,\xi(t)]$ was additionally superposed on $\boldsymbol{E}(t)(\boldsymbol{\xi}\,//\,\boldsymbol{E})$; thus, a fluctuating sinusoidal field was applied across the NLC sample cells. We used *colored noise* characterized by its intensity V_N and correlation time $\tau_N[= 1/(2\pi f_c)]$; f_c indicates a cutoff frequency of noise that is determined by the low-pass filters of a synthesizer (7075, Hioki), at which the power output becomes half the passband power $P(f < f_c)$. Three typical kinds of cells were prepared for this study [26]: a planar alignment cell [PL, $\boldsymbol{n_0} = (1,0,0)$ for the initial director of NLCs], a homeotropic alignment cell [HO,$\boldsymbol{n_0} = (0, 0, 1)$], and a π/2-twisted alignment cell (TW,$\boldsymbol{n_0} = [n_x(z),n_y(z),0]$, $n_x^2 + n_y^2 = 1$). In this paper, the results obtained in TW are mainly presented except for Fig. 6. The (deterministic) ac voltage $V = d\sqrt{\langle E^2(t)\rangle}$ and its frequency f (for driving EC), and the (stochastic) noise intensity $V_N = d\sqrt{\langle \xi^2(t)\rangle}$ and its cutoff frequency f_c (i.e., the correlation time τ_N) were used as the main control parameters. All measurements were carried out at a stable temperature ($T = 28 \pm 0.2\,^\circ$C) using

an electrothermal control system (TH-99, Japan Hightech). The details of our experiments were explained in our previous papers [25].

III. RESULTS AND DISCUSSION

A. Noise-intensity-dependent pattern evolution and threshold shift

First, to understand better the noise impact that can stabilize or destabilize EC [23–25], let us see an actual pattern evolution in the course of increasing noise intensity V_N. A typical EC pattern, the so-called Williams domain [WD, Fig. 1(a)], occurred slightly above a threshold ac voltage $V_c(V_N = 0)$ [26]. Applying noise and increasing its intensity V_N to the WD (at a fixed $V = 7.1\,\mathrm{V} > V_c = 6.6\,\mathrm{V}$), an unusual successive pattern evolution was observed (Fig. 1). The noise ($V_N = 7.8\,\mathrm{V}$) suppresses the preexisting ac-driven EC (WD); consequently, the EC disappears because of the stabilization effect of noise [Fig. 1(b)]. Inexplicably, the EC reappears at $V_N = 12.7\,\mathrm{V}$ because of the destabilization effect of noise [Fig. 1(c)]; moreover, appearance of defects [Fig. 1(d)] and fluctuating WD (FWD) [Fig. 1(e)] follows with increasing V_N. The important point is that a rest state [Fig. 1(b), amplitude $A \sim 0$, see below] appears at a certain appropriate noise intensity (V_N^*), at a level not too small and not too large. In other words, an ISR-like phenomenon exists in the present EC system. In the usual pattern evolutions in the course of increasing ac voltage V [27] or noise intensity V_N [28], the reentrance of the WD after the rest state has never been found above V_c. To understand the phenomenon more clearly, we need to consider the characteristic of noise, that is to say, colored noise and white noise. In fact, the unusual pattern evolution (Fig. 1) was able to be obtained only by using appropriate colored noises (e.g., $f_c = 500\,\mathrm{Hz}$ in this experiment) [13].

Next, by taking into account the cutoff frequency f_c of noise, the threshold ac voltage V_c was measured with increasing V_N; namely, the pattern evolution (Fig. 1) was examined in the variation of V_c. Figure 2 shows V_N-dependent V_c with respect to f_c. The low-f_c colored noises ($f_c = 200, 500\,\mathrm{Hz}$) give rise to a completely different function $V_c(V_N)$ in comparison with that at $f_c = 1\,\mathrm{kHz}$ (and white noise). In particular, $V_c(V_N)$ shows a bell-shaped curve for $f_c = 500\,\mathrm{Hz}$, whereas it monotonically decreases ($f_c = 200\,\mathrm{Hz}$) or increases ($f_c = 1\,\mathrm{kHz}$) with increasing V_N. A maximal voltage $V_c(f_c = 500\,\mathrm{Hz})$ appears to be realized around a certain intensity $V_N^* \sim 9.0\,\mathrm{V}$, at which the rest state can occur even if a fixed $V[> V_c(V_N = 0)]$ is applied [Fig. 1(b)]. Namely, for appropriate colored noises (e.g., $f_c = 500\,\mathrm{Hz}$), a peak of the response of the system (i.e., a maximal stabilization effect of noise) is found at an optimal noise intensity V_N^*. Above $V_N \sim 12.5\,\mathrm{V}$, the stabilization effect of noise is switched into a destabilization effect [$V_c < V_c(V_N = 0) = 6.6\,\mathrm{V}$]; $V_c(V_N > 12.5\,\mathrm{V})$ monotonically decreases as it does for $f_c = 200\,\mathrm{Hz}$, and the reentrance of WD is realized above $V_N = 12.5\,\mathrm{V}$ if a fixed V is applied [Fig. 1(c)]. Similar threshold behaviors [such as $V_c(V_N, f_c = 500\,\mathrm{Hz})$] have occasionally been reported in past studies [25,29]. However, they should be differentiated from the present result showing the reentrance of WD for ISR, because noise-dominated patterns [25] or complicated patterns [29] were found instead of the WD reentered.

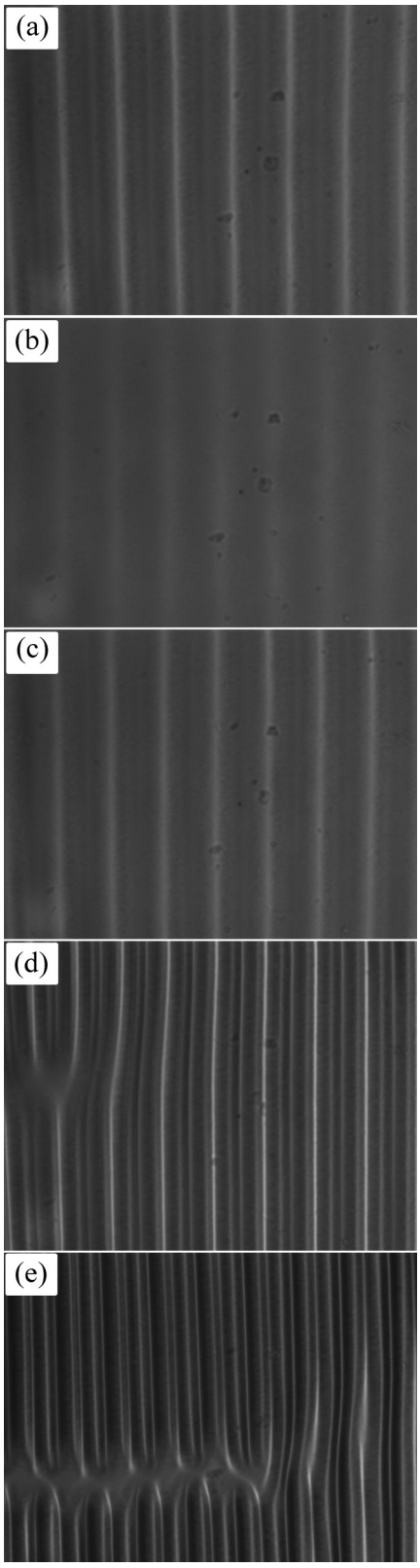

FIG. 1. Pattern evolution with increasing noise intensity $V_N(f_c = 500\,\mathrm{Hz}) = 0$ (a); 7.8 V (b); 12.7 V (c); 13.5 V (d); 17.4 V (e). The amplitude A of Williams domain (WD, at a fixed $V = 7.1\,\mathrm{V}$ and $f = 30\,\mathrm{Hz}$) is varied by V_N; A first decreases to zero [$A \sim 0$ at (b)], and then recovers (c) with increasing V_N. The size of each frame is $X \times Y = 640\,\mathrm{pixels} \times 480\,\mathrm{pixels}$ ($= 0.421\,\mathrm{mm} \times 0.316\,\mathrm{mm}$).

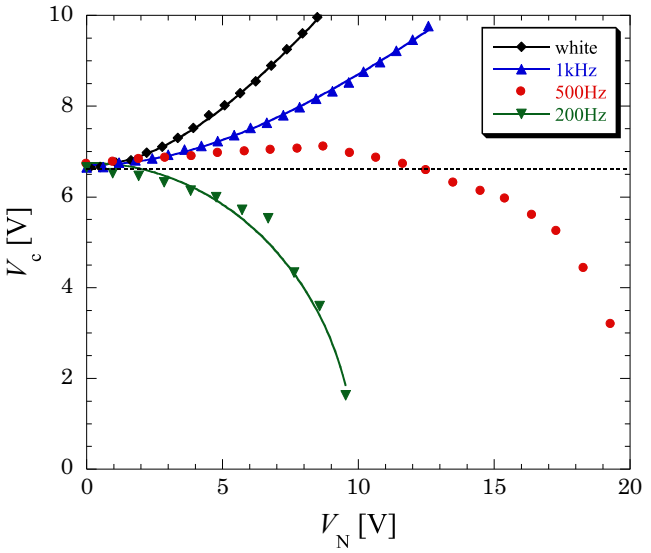

FIG. 2. Noise intensity V_N-dependent threshold voltage V_c for WD with respect to the cutoff frequency f_c of noise. The solid lines were calculated by the typical relationship between V_c and V_N: $V_c^2 = V_{c0}^2 + b(f_c)V_N^2$ [24,25]. Here, V_{c0} and b indicate a threshold voltage for WD ($V_N = 0$) and a sensitivity of WD to noise, respectively. In the case of $f_c = 500$ Hz, the linear relationship is inapplicable to the complicated behavior. See also Fig. 1.

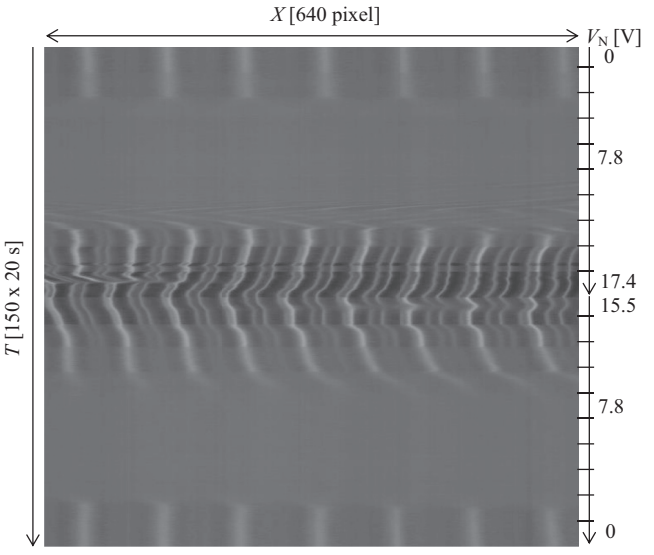

FIG. 3. Spatiotemporal plot for the pattern evolution (i.e., the amplitude $\boldsymbol{A}$ of one-dimensional images of patterns) with increasing or decreasing noise intensity $V_N(f_c = 500$ Hz). An arbitrarily selected one-dimensional line (X) in WD [at a fixed $V = 7.1$ V and $f = 30$ Hz, Fig. 1(a)] was successively placed in order of time T (with step increase of V_N). As seen in Fig. 1, WD ($\boldsymbol{A} \neq 0$) disappears ($\boldsymbol{A} \sim 0$ around $V_N = 7.8$ V) and reappears ($\boldsymbol{A} \neq 0$) near $V_N = 12.0$ V) with increasing V_N ($0 \rightarrow 17.4$V); the reverse variation of $\boldsymbol{A}$ is also obtained with decreasing $V_N(17.4\,\text{V} \rightarrow 0)$. For each value of V_N, the measurement time is 150 s (i.e., $X \times T = 640$ pixels $\times$ 30 pixels); total $X \times T = 640$ pixels $\times$ 600 pixels(= 0.421 mm $\times$ 3000 s).

Moreover, the result is qualitatively different from conventional SR expecting enhancement of the WD in Fig. 1(b) [i.e., the increase of $\boldsymbol{A}$ and a decrease of the intensity of the periodic signal (showing a minimal V_c at V_N^* in Fig. 2)]. Accordingly, this phenomenon can be considered as a kind of ISR that is first found in the EC system [12–15]. It is important that *moderately* colored noises (e.g., $f_c = 500$ Hz in this experiment) can induce such an ISR. On the other hand, the behavior of $V_c(V_N)$ for the noise ($f_c = 1$ kHz) is similar to that for white noise ($f_c \rightarrow \infty : \sim 500$ kHz in our experimental limitation) [i.e., $b > 0$ in the relationship $V_c^2 = V_{c0}^2 + b(f_c)V_N^2$], but, $b < 0$ for the extremely colored noise ($f_c = 200$ Hz) [24,25]. In a case sufficiently above or below a certain characteristic $f_c^\dagger$ ($\sim$500 Hz in this experiment), the noises simply serve as stabilization ($b > 0$ for $f_c > f_c^\dagger$) or destabilization ($b < 0$ for $f_c < f_c^\dagger$) effects on the EC. The noise with moderate cutoff frequency (around $f_c^\dagger$) inducing ISR has been overlooked in the past studies because of experimental limitation (e.g., limited variations of f_c) [25]. In this study, $f_c^\dagger$ was able to be found at an appropriate temperature of the system (i.e., for the NLC) which delicately influences $V_c(f_c)$; the dependence of material constants (e.g., conductivity or permittivity) on $f_c^\dagger$ will be examined in future studies.

B. Spatiotemporal plots and amplitude variations of electroconvection

To show more clearly the appearance of the rest state (i.e., the evidence of ISR) [Fig. 1(b)], we measured spatiotemporal variations of EC in the course of increasing V_N. In Fig. 3, an arbitrarily selected one-dimensional image (X) in an EC pattern (at a fixed $V = 7.1$ V) was successively placed in order of time T (with step increase of V_N); at a value of V_N, the amplitude $\boldsymbol{A}(V_N)$ of the EC was successively measured for 150 s (with an identical time interval $\Delta t = 1$s). For $T = 0$ to 1500 s (increasing V_N from 0 to 17.4 V), the amplitude $\boldsymbol{A}$ (the maximal brightness difference in the pattern) of the EC smoothly decreases to zero ($\boldsymbol{A} \rightarrow 0$) and then smoothly recovers ($\boldsymbol{A} > 0$); after this, it fluctuates spatially and temporally owing to moving defects around $V_N = 16.0$ V. Also, decreasing V_N from 17.4 to 0 V, the reverse variation of $\boldsymbol{A}$ is found. This result is well consistent with the pattern evolution (Fig. 1). In addition, the spatiotemporal plot for each V_N depicted in a much longer time shows more detailed behaviors of $\boldsymbol{A}$, as shown in Fig. 4. Spatially and temporally stable plots [Figs. 4(a) and 4(b)] can be realized, whereas spatially or temporally unstable ones [Figs. 4(c) and 4(d)] have also appeared; the rest state [Fig. 1(b)] was also observed for longer time (i.e., it is not a transient state), although its plot is not given in Fig. 4.

If the rest state and the reentrance of the WD are not found, the noise plays a role as a pure additional increment of voltage (i.e., an average power effect) rather than its irregular field effect because the similar plots (Fig. 4) can be also obtained by increasing pure ac voltage [28]. In this study, however, the rest state ($\boldsymbol{A} = 0$) always appears at optimal noise levels with moderate cutoff frequencies (i.e., around V_N^* and $f_c^\dagger$).

Moreover, by changing f_c, the brightness intensity $\boldsymbol{I}(X_i)$ of the WD was directly measured at a fixed point X_i (in a one-dimensional image (X); see Figs. 3 and 4) which indicates the peak intensity I_{max} [see Fig. 7(a)]. A normalized intensity $\boldsymbol{I}_0$ [i.e.,$\boldsymbol{I}_0 = 1$ at $V_N = 0$ and $\boldsymbol{I}_0 = 0$ at $V_N = V_N^*$] after averaging $[(1/m)\sum_i I(X_i)]$ is given in Fig. 5 (m is

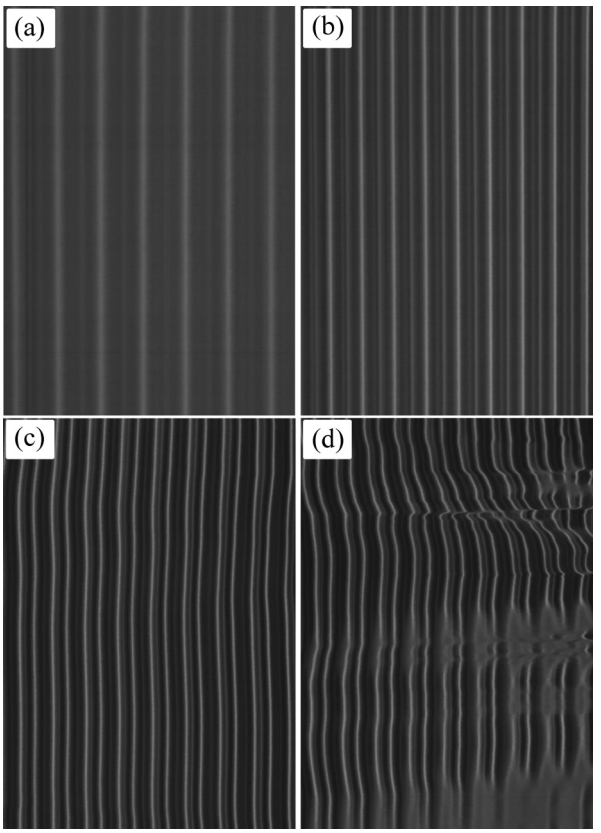

FIG. 4. Spatiotemporal plots for the pattern evolution (i.e., XT plots) at a fixed $V = 7.1\,\mathrm{V}, f = 30\,\mathrm{Hz}$, and $V_\mathrm{N}(f_\mathrm{c} = 500\,\mathrm{Hz}) = 0$ (a); 13.5 V (b); 15.5 V (c); 17.4 V (d). The size of each plot is $X \times T = 640\,\mathrm{pixels} \times 900\,\mathrm{pixels}(= 0.421\,\mathrm{mm} \times 900\,\mathrm{s})$.

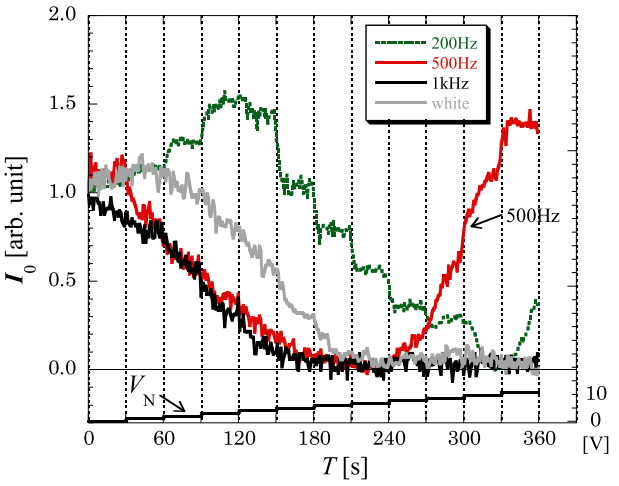

FIG. 5. A normalized brightness-intensity ($\boldsymbol{I}_0$) variation with increasing noise intensity V_N with respect to the cutoff frequency f_c (at a fixed $V = 7.1\,\mathrm{V} > V_\mathrm{c} = 6.6\,\mathrm{V}$, and $f = 30\,\mathrm{Hz}$). $\boldsymbol{I}_0$ was measured at fixed points on X (a one-dimensional image; see Figs. 3 and 4) which indicate the peak intensity I_max [see Fig. 7(a)]; it was measured for 30 s at each fixed V_N [with steplike increase ($0 \rightarrow 10.6\,\mathrm{V}$)]. Notice that there exists $\boldsymbol{I}_0 \sim 0$ in the reversed bell-shaped variation for $f_\mathrm{c} = 500\,\mathrm{Hz}$; it corresponds to Fig. 1(b). For $f_\mathrm{c} = 200\,\mathrm{Hz}, \boldsymbol{I}_0(T > 120\,\mathrm{s})$ should be neglected because it behaves like that because of appearance of defects [i.e., change of the points $X(I_\mathrm{max})$] at larger V_N.

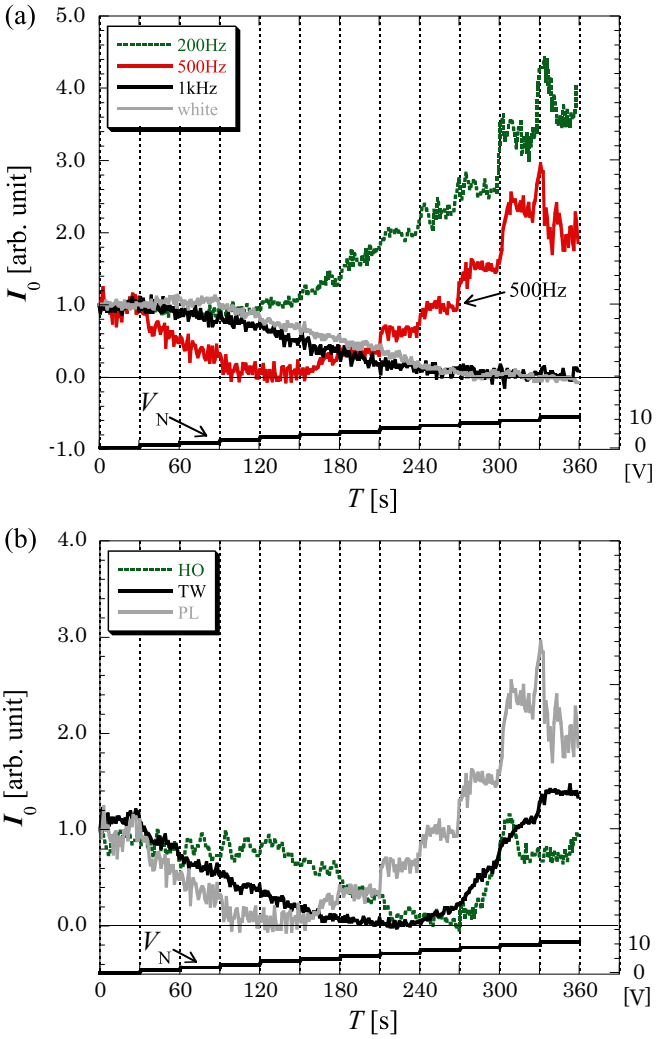

FIG. 6. (a) A normalized brightness-intensity ($\boldsymbol{I}_0$) variation with steplike increase of V_N with respect to the cutoff frequency f_c at a PL cell and (b) its comparison for three different cells (TW: twist cell, HO: homeotropic cell, PL: planar cell) at an identical $f_\mathrm{c} = 500\,\mathrm{Hz}$. Notice that there exists $\boldsymbol{I}_0 \sim 0$ at a certain V_N^* for each different cell.

the number of I_max in X). In the course of the steplike increase of V_N, $\boldsymbol{I}_0$ shows different behavior with respect to f_c (see also Fig. 2). Obviously, a reversed bell-shaped $\boldsymbol{I}_0(T)$ [i.e., $\boldsymbol{I}_0(V_\mathrm{N})$] appears for $f_\mathrm{c} = 500\,\mathrm{Hz}$, whereas $\boldsymbol{I}_0$ monotonically decreases to zero for $f_\mathrm{c} = 1\,\mathrm{kHz}$ and white noise. On the other hand, $\boldsymbol{I}_0(f_\mathrm{c} = 200\,\mathrm{Hz})$ increases with increasing V_N ($< 4\,\mathrm{V}$ for $T < 120\,\mathrm{s}$); above $4\,\mathrm{V}(T > 120\,\mathrm{s})$, it decreases owing to appearance of defects or fluctuating rolls, which is not related to the noise effect for the ISR. Such $\boldsymbol{I}_0(T, f_\mathrm{c})$ was reproduced in a PL cell, as shown in Fig. 6(a); notice that $\boldsymbol{I}_0(f_\mathrm{c} = 500\ \mathrm{Hz})$ shows the discriminable behavior in comparison with other $\boldsymbol{I}_0(f_\mathrm{c} \neq 500\ \mathrm{Hz})$. Furthermore, we can compare such $\boldsymbol{I}_0(f_\mathrm{c} = 500\,\mathrm{Hz})$ in terms of the types of cells (HO, TW, and PL) in Fig. 6(b). The rest state ($\boldsymbol{I}_0 = 0$) appears in the course of increasing V_N, although the values V_N^* (for $\boldsymbol{I}_0 = 0$) are dependent on the types of cells. This reversed bell-shaped $\boldsymbol{I}_0(V_\mathrm{N})$ is crucial evidence of ISR.

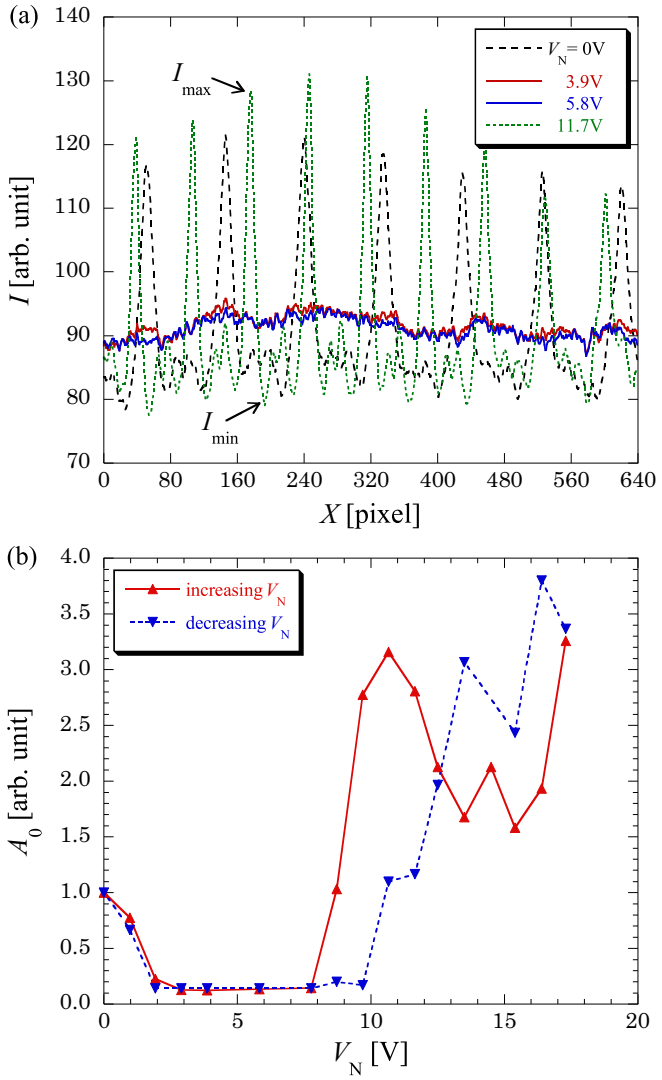

FIG. 7. (a) Brightness intensity $\boldsymbol{I}(X)$ in a one-dimensional image ($X = 640$ pixels) at various noise intensities $V_N(f_c = 500\,\text{Hz})$. (b) Amplitude variation with increasing and decreasing V_N. A normalized amplitude $\boldsymbol{A}_0$ was calculated for some peaks after averaging the intensity difference $(I_{max} - I_{min})$ at each peak point. $I(X)$ for $V_N = 3.9$ and 5.8 V corresponds to the rest state (i.e., no EC). $\boldsymbol{A}_0$ shows a reversed bell-shaped variation in V_N (with a background error $\boldsymbol{A}_0 = 0.06$); this coincides with the pattern evolution (Fig. 1) and the spatiotemporal plot (Fig. 3).

C. Noise-intensity-dependent amplitude of electroconvection

Finally, we directly examined the dependence of a normalized amplitude $\boldsymbol{A}_0$ of EC on V_N [after enough waiting time (120 s) at each V_N]. From the profile of the brightness intensity $\boldsymbol{I}(X)$ in a one-dimensional image [Fig. 7(a)], $\boldsymbol{A}_0(V_N)[= \{\boldsymbol{A}(V_N) - \boldsymbol{A}(V_N^*)\}/\{\boldsymbol{A}(V_N = 0) - \boldsymbol{A}(V_N^*)]$ was calculated at various noise intensities (V_N) [Fig. 7(b)]. For example, as $\boldsymbol{I}(X, V_N = 11.7\,\text{V})$ has nine peaks (I_{max}), $\boldsymbol{A}(V_N) = (1/9)\sum_i I^i_{max}(V_N) - I^i_{min}(V_N)$. In Fig. 7(a), $I(X)$ for $V_N = 3.9$ and 5.8 V corresponds to the rest state [i.e., $\boldsymbol{A}_0 = 0$ for no EC in Fig. 1(b)]. In Fig. 7(b), $\boldsymbol{A}_0$ (= 1 at $V_N = 0$) monotonically decreases to $\boldsymbol{A}_0 \sim 0$ (i.e., the rest state) with increasing V_N, and then it increases with V_N after no variation $\boldsymbol{A}_0(2\,\text{V} < V_N < 8\,\text{V}) \sim 0$. Namely, $\boldsymbol{A}_0(V_N)$ shows again the reversed bell-shaped behavior. However, beyond 10 V, $\boldsymbol{A}_0$ violently fluctuates because of the motion of defects. Moreover, the reverse variation of $\boldsymbol{A}_0$ was also found (with a small hysteresis) by decreasing V_N [30]. These results are consistent with the pattern evolutions described above (Figs. 1 and 3) as evidence of ISR. More importantly, the present ISR strongly depends on the correlation time τ_N of noise (i.e., the cutoff frequency f_c of noise) [13].

From the experimental results, let us speculate about a possible explanation of the ISR appearing in the EC system. Considering a relationship between the charge relaxation time τ_σ of the EC and τ_N (or f_c) of the noise that plays a crucial role in the stability [25], the ISR seems to be induced by colored noises with appropriate $\tau_N[= \tau_N(\tau_\sigma)]$ and V_N. Thus, appropriately colored noises ($f_c \sim f_c^\dagger; b \sim 0$) crossing between extremely colored ($f_c < f_c^\dagger; b < 0$) and whitelike ($f_c > f_c^\dagger; b > 0$) noises can give rise to the ISR. Moreover, the noise appears to simply serve as an extremely colored one

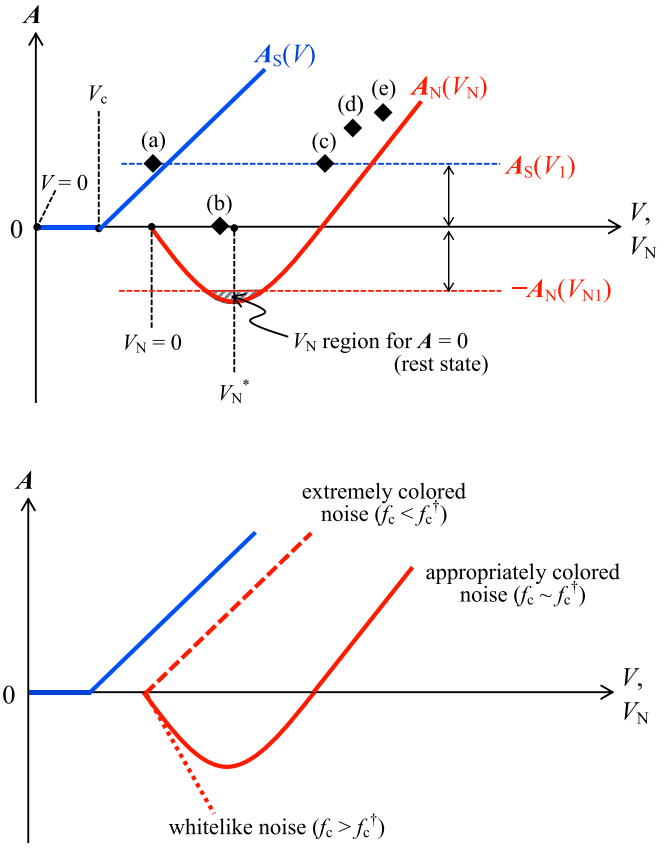

FIG. 8. Schematic diagram for the inverse stochastic resonance (ISR). If noise-induced amplitude can be supposed in a linear relation $\boldsymbol{A}(V + V_N) = \boldsymbol{A}_S(V) + \boldsymbol{A}_N(V_N)$, the present ISR is possible (top panel). In the region of noise intensity V_N indicating $|\boldsymbol{A}_N(V_N)| > \boldsymbol{A}_S(V)$, the rest state [i.e., no EC, Fig. 1(b)] can be realized. The ♦ symbols (a)–(e) mean $\boldsymbol{A}$ for Figs. 1(a)–1(e), respectively; $\boldsymbol{A}_S(V_1)$ represents a constant $\boldsymbol{A}$ for a fixed V_1 (e.g., = 7.1 V in Fig. 1). Compare $\boldsymbol{A}_N(V_N)$ with respect to f_c (bottom panel). No ISR is expected for extremely colored noises ($f_c < f_c^\dagger$) and whitelike noises ($f_c > f_c^\dagger$); it will be found that $\boldsymbol{A}(V + V_N)$ monotonically decreases ($f_c > f_c^\dagger$) or increases ($f_c < f_c^\dagger$) with increasing V_N.

($b < 0$: decreasing V_c) in small noise intensity V_N ($< V_N^*$), whereas it serves as a whitelike one ($b > 0$: increasing V_c) in large noise intensity V_N ($\gg V_N^*$).

To better understand the above-mentioned facts on f_c and V_N, our speculation is schematized in Fig. 8. Considering pure ac- and noise-induced amplitudes [$A_S(V)$ and $A_N(V_N)$] in our previous results [31], the ISR is possible in the assumption that appropriately colored noises ($f_c \sim f_c^\dagger$) behave like $A_N(V_N)$ in Fig. 8, satisfying a linear relation [$A(V + V_N) = A_S(V) + A_N(V_N)$]; $A(V + V_N) < 0$ for the rest state ($A = 0$). For example, for $A(V_1 + V_N^*) = A_S(V_1) - A_N(V_N^*) < 0$, the rest state arises [$A = 0$ near (b) in Fig. 8]. However, the ISR cannot be expected for extremely colored noises ($f_c < f_c^\dagger$) and whitelike noises ($f_c > f_c^\dagger$). In the region for (imaginary) $A_N(f_c^\dagger) < 0$ (implying oppression intensity to EC), it seems that the noise interacts more delicately with the details of EC (e.g., viscoelastic properties or other relaxation times [32]) for the occurrence of the ISR. The reason why $A_N(f_c^\dagger)$ behaves in this way still remains as open problems. Under these specific conditions of the system (V, V_N, f_c, and f), the ISR may be observed and controlled. Intuitively, such an ISR may not be explained by the conventional assumption for SR for which a double minimum potential function exists in the systems [2].

IV. SUMMARY AND CONCLUSION

We have discovered a kind of inverse stochastic resonance (ISR) in a spatially extended system for which ac-driven EC in an NLC is employed. To elucidate the ISR, the pattern evolution and threshold variation have been examined in the course of increasing noise intensity V_N. Moreover, by measuring the amplitude of EC in a one-dimensional image (X) and the brightness intensity at one point (X_i), the ISR has been investigated. For appropriate colored noises with moderate cutoff frequency f_c (or the correlation time τ_N of noise) and optimal intensity V_N, a maximal threshold ac voltage $V_c(V_N)$ and a minimal amplitude $A(V_N)$ have been found. Therefore, continuously increasing V_N, a typical EC (Williams domain with a normalized amplitude $A_0 = 1$ at $V_N = 0$) evolves into the rest state ($A_0 = 0$), and then reenters into the EC ($A_0 = 1$); eventually, it develops into secondary EC($A_0 > 1$) such as defect chaos and fluctuating Williams domains. Until now such a successive pattern evolution in the EC system could not be found, since the characteristic of colored noise (i.e., f_c or τ_N) has been overlooked. Under specific conditions of the system such as the correlation time and intensity of the external noise and the intrinsic times (e.g., charge relaxation time τ_σ) of EC, the ISR has been discovered. Like the well-known stochastic resonance (SR), ISR may be a universal characteristic of nonlinear systems [30]. For noise-controlled applications, ISR has a different possibility in comparison with the normal SR achieving output enhancement. If the output of systems includes a kind of side effect (e.g., in drug or radiation therapy), one may consider ISR rather than SR. In the case of affective disorders addressed in neuropsychiatry, noise stimuli can minimize the probability of the sensitization of the disease [33]; in that case, ISR may be required for practical treatments. By using both phenomena which can enhance (SR) or inhibit (ISR) the output of systems, noise-controlled applications are expected in a wider variety of fields and in more different ways.

ACKNOWLEDGMENT

This study was partly supported by JSPS KAKENHI (Grant No. 15K05215).

[1] W. Horsthemke and R. Lefever, *Noise-Induced Transitions* (Springer-Verlag, Berlin, 1984).
[2] J. Garcia-Ojalvo and J. M. Sancho, *Noise in Spatially Extended Systems* (Springer-Verlag, New York, 1999).
[3] F. Sagués, J. M. Sancho, and J. García-Ojalvo, Rev. Mod. Phys. **79**, 829 (2007).
[4] A. A. Green, M. Berman, P. Switzer, and M. D. Craig, IEEE Trans. Geosci. Remote Sens. **26**, 65 (1988).
[5] Y. Dong and S. Xu, IEEE Signal Process. Lett. **14**, 193 (2007).
[6] J. K. Douglass, L. Wilkens, E. Pantazelou, and F. Moss, Nature **365**, 337 (1993).
[7] S. M. Bezrukov and I. Vodyanoy, Nature **378**, 362 (1995).
[8] R. Benzi, A. Sutera, and A. Vulpiani, J. Phys. A **14**, L453 (1981); C. Nicolis, Tellus **34**, 1 (1982); R. Benzi, J. Stat. Mech. (2009) P01052.
[9] L. Gammaitoni, Rev. Mod. Phys. **70**, 223 (1998).
[10] X.-J. Zhang, H. Qian, and M. Qian, Phys. Rep. **510**, 1 (2012).
[11] L. S. Borkowski, Phys. Rev. E **82**, 041909 (2010).
[12] B. Gutkin, J. Jost, and H. C. Tuckwell, Naturwissenschaften **96**, 1091 (2009); H. C. Tuckwell, J. Jost, and B. S. Gutkin, Phys. Rev. E **80**, 031907 (2009); H. C. Tuckwell and J. Jost, Physica A **391**, 5311 (2012).
[13] D. Guo, Cognit. Neurodyn. **5**, 293 (2011).
[14] M. Uzuntarla, Phys. Lett. A **377**, 2585 (2013).
[15] M. Uzuntarla, J. R. Cressman, M. Ozer, and E. Barreto, Phys. Rev. E **88**, 042712 (2013).
[16] A. L. Hodgkin and A. F. Huxley, J. Physiol. **117**, 500 (1952).
[17] P. Jung and G. Mayer-Kress, Phys. Rev. Lett. **74**, 2130 (1995).
[18] J. M. G. Vilar and J. M. Rubí, Phys. Rev. Lett. **78**, 2886 (1997).
[19] T. Taneike and Y. Shiwa, J. Phys.: Condens. Matter **11**, L147 (1999).
[20] H. Wang, Phys. Rev. Lett. **93**, 154101 (2004).
[21] A. Hutt, Europhys. Lett. **84**, 34003 (2008).
[22] L. Barbini, I. Bordi, and K. Fraedrich, Eur. Phys. J. Plus **129**, 190 (2014).
[23] S. Kai, T. Kai, M. Takata, and K. Hirakawa, J. Phys. Soc. Jpn. Lett. **47**, 1379 (1979); H. Brand and A. Schenzle, J. Phys. Soc. Jpn. **48**, 1382 (1980); S. Kai, H. Fukunaga, and H. Brand, J. Phys. Soc. Jpn. Lett. **56**, 3759 (1987).
[24] T. Kawakubo, A. Yanagita, and S. Kabashima, J. Phys. Soc. Jpn. **50**, 1451 (1981).
[25] J.-H. Huh, A. Kuribayashi, and S. Kai, Phys. Rev. E **80**, 066304 (2009); J.-H. Huh, *ibid.* **84**, 025302(R) (2011); J.-H. Huh and S. Kai, J. Phys. Soc. Jpn. Lett. **83**, 063601 (2014); J.-H. Huh, Phys. Rev. E **92**, 062504 (2015); J. Phys. Soc. Jpn. **85**, 024002 (2016).

[26] L. M. Blinov, *Electro-optical and Magneto-optical Properties of Liquid Crystals* (The Universities Press (Belfast) Ltd., Belfast, UK, 1983).
[27] J.-H. Huh, Y. Hidaka, A. G. Rossberg, and S. Kai, Phys. Rev. E **61**, 2769 (2000).
[28] J.-H. Huh, J. Phys. Soc. Jpn. Lett. **76**, 033001 (2007).
[29] H. Amm, U. Behn, T. John, and R. Stannarius, Mol. Cryst. Liq. Cryst. **304**, 525 (1997).
[30] B. Gutkin, J. Jost, and H. Tuckwell, Neurocomp08 (2008), https://hal.archives-ouvertes.fr/hal-00331543.
[31] J.-H. Huh, J. Phys. Soc. Jpn. Lett. **79**, 123602 (2010).
[32] M. Dennin, M. Treiber, L. Kramer, G. Ahlers, and D. S. Cannell, Phys. Rev. Lett. **76**, 319 (1996).
[33] M. T. Huber, H. A. Braun, and J. -C. Krieg, Int. J. Bifurcation Chaos **14**, 635 (2004).